Zn2+ -Schiff's base Complex as an "On-Off-On" Molecular Switch and a Fluorescence Probe for the Cu2+ and Ag+ ions

Shaaban Elroby (skamel@kau.edu.sa)
King Abdulaziz University https://orcid.org/0000-0002-6739-824X
Bashair Abdullah Banaser
King Abdulaziz University
Saadullah G Aziz
King Abdulaziz University
Abdesslem Jedidi
King Abdulaziz University
Walid I Hassan
King Abdulaziz University
Osman I Osman
King Abdulaziz University

Research Article

Keywords: Photoinduced Electron Transfer (PET), fluorescence probe molecular switch, Schiff base, Density Functional Theory (DFT), Time Dependent Density Functional Theory (TDDFT)

Posted Date: October 22nd, 2021

DOI: https://doi.org/10.21203/rs.3.rs-974764/v1

Version of Record: A version of this preprint was published at Journal of Fluorescence on January 18th, 2022. See the published version at https://doi.org/10.1007/s10895-021-02864-4.

Abstract

The present study presents a thorough theoretical analysis of the electronic structure and conformational preference of the Schiff's base ligand N,N-bis(2-hydroxybenzilidene)-2,4,6-trimethyl benzene-1,3-diamine (H_2L) and its metal complexes with Zn^{2+}, Cu^{2+} and Ag^{+} ions. The study aims to investigate the behavior of H_2L and the binuclear Zn^{2+} complex (**1**), as fluorescent probes for the detection of metal ions (Zn^{2+}, Cu^{2+} and Ag^{+}) using Density Functional Theory (DFT) and Time Dependent Density Functional Theory (TDDFT). The six conformers of the H_2L ligand were optimized using B3LYP/6-311++G** level of theory, while the L^{-2}-metal complexes were optimized by applying B3LYP functional with LANL2DZ/6-311++G** mixed basis set. The gas-phase and solvated Enol-cis isomer (E-cis) was found to be the most stable species. The absorption spectra of E-cis isomer and its metal complexes were simulated using B3LYP, CAM-B3LYP, M06-2X and ωB97X functionals with a 6-311++G** basis set for C, O, N and H atoms and LANL2DZ basis set for the metal ions (Zn^{2+}, Cu^{2+} and Ag^{+}). The computational results of B3LYP functional were in excellent agreement with the experimental ones. Hence, it has been adopted for performing the emission calculations. The results indicated that, the metal complex (**1**) can act as a fluorescent chemosensor, for the detection of Ag^{+} and Cu^{2+} ions through the mechanism of the Intermolecular Charge Transfer (ICT) and as a molecular switch "On-Off-On" via the replacement of Cu^{2+} by Ag^{+} ions, as proved experimentally.

1. Introduction

Due to their operational simplicity, high sensitivity, and high response speed, fluorescent probes have been widely applied in diverse fields such as chemical biology, medicinal chemistry, analytical chemistry, and molecular biology [1]. The employment of fluorescent probes has revolutionized our understanding of several physiological or pathological processes and has provided effective sensing protocols for the detection of harmful species that may have been released into the environment (aqueous and gaseous). The fluorescent probes use either specific host-guest interactions or selective chemical reactions to affect changes in the fluorescence properties. If the binding between the host and guest is non-covalent and reversible, then the fluorescent probe is known as a chemosensor. Alternatively, if the interaction between the host and guest leads to an irreversible chemical reaction, then the fluorescent probe is known as a chemodosimeter [2].

The chemical compounds with azomethine (-CH=N-) groups are called Schiff's bases. They are excellent classes of ligands and enjoyed a popular use in coordination chemistry because they form coordinate bonds with metal ions to produce coordination metal complexes. The metal complexes incorporating Schiff's bases have played important roles in the advancement of inorganic chemistry. They were discovered by Hugo Schiff's (Germanist) [3]. Schiff's bases have considerable chemical and biological importance because of their easy method of preparation, excellent chelating ability and synthetic flexibility [4–5].

Schiff's bases show photochromism and thermochromism in the solid state through proton transfer from the hydroxyl (O) atom to the imine (N) atom [6–9]. Salicylideneanilines Schiff's bases (SAS) are dynamical systems, usually referred as molecular switches [10] that exhibit thermochromism [11–15], photochromism [12–13, 16–19], solvatochromism [13, 20, 21], and nonlinear optical (NLO) switching properties [21–24]; both in solution and solid state. The SAS molecules can undergo keto-enol tautomerism when triggered by light or temperature changes [25–26]. This behavior is shown by their Cis and Trans isomers, which are characterized by one or/and two intramolecular H-bonding. The Schiff's bases probes possess are characterized by —OH (phenolic) and N— (imine) functional groups being close to each other and hence become excellent hydrogen donor and acceptor sites, respectively, for constructing Excited-State Intramolecular Proton-Transfer (ESIPT) entities that can be used as metal ions specific probes [27–29].

Among the most important molecules used, there is a new Schiff's base ligand N,N-bis(2-hydroxybenzilidene)-2,4,6-trimethyl benzene-1,3-diamine (H_2L) [1]. It binds with rare earth metal ions such as zinc ion (Zn^{2+}), copper ion (Cu^{2+}) and silver ion (Ag^{+}) (See Scheme 1). Despite the existence of numerous applications for such molecules, the geometry and the exact nature of the cation binding are not fully investigated.

In the present work, based on the experimental study of the Schiff's base and its metal complexes [1]; a Density Functional Theory (DFT) computational study was performed to complete the experimental detection of the Ag^{+} ion and the Cu^{2+} ion through the fluorescence phenomenon by using the binuclear Zn^{2+} complex as a molecular switch.

Therefore, this study is designed to answer a question related to the difference in the fluorescence intensity of these metal complexes by explaining the mechanisms that lead to these fluorescence responses through a DFT computational study. Moreover, the classification of molecules according to the type it assumes as a fluorescence probe, i.e. a chemosensor or a chemodosimeter, is also tackled.

Finally, we aim to investigate the reason for the difference in the fluorescence intensity of the substrates by applying extensive theoretical studies of the ground and excited electronic states of the ligand conformers (H_2L) and its Zn^{2+}, Cu^{2+} and Ag^{+} metal ions complexes.

2. Computational Details

All the calculations were performed using the G09 program package [30]. All the possible conformers of the ligand (H_2L) were optimized using B3LYP/6-311++G** [31-33] level of theory. The frequency calculations were performed to confirm global minima or transition states on the potential energy surfaces by having zero or one imaginary frequency, respectively. The ligand-metal complexes were optimized by using B3LYP functional with a 6-311++G** basis set for all atoms except the metal ions, for which LANL2DZ basis set was used. In addition, the Zn-complex was subjected to further confirmation

and validation using more functionals; namely CAM-B3LYP, M06-2X and ωB97X. The binding energies (E_{BE}) of the complexes were calculated by the equation:

$$E_{BE} = E_{AB} - (E_A + n\,E_B)$$

where E_{AB} is the total energy of the geometry complex, E_B is the corresponding total energy for the optimized ligand B, n is the number of ligands in the complex and E_A is the total energy of single point energy calculation for metal (A) using the same multiplicity as in the complex case [34]. The absorption and emission UV-VIS spectra of the E-cis isomer were simulated using TDDFT [35] method at B3LYP/6-311++G** level of theory; while the metal complexes were studied by B3LYP/LANL2DZ/6-311++G**level of theory. These calculations were intended for investigating the electronic properties, such as HOMO–LUMO energies, dipole moment, absorption-emission wavelengths and oscillator strengths.

The energy gap calculation is very important for investigating the molecular orbitals that result from the chemical reactions or the electronic excitation:

$$E_{gap}\,(eV) = E_{LUMO}\,(eV) - E_{HOMO}\,(eV)$$

For both DFT and TDDFT calculations, the gas-phase calculations were carried out at 298 K and 1 atm. The solvent effect was studied using conductor-like polarizable continuum model (CPCM) [36,37] with methanol as a solvent at 298 K.

3. Results And Discussion

3.1 Isomerization and Tautomerization of Ligands

Figure 1 depicts the atom numbering of the optimized structure of gas-phase H_2L ligand which was adopted from the X-ray diffraction crystal structure [1]. It has the molecular formula $C_{23}H_{42}N_2O_2$. Theoretically, the structures of the H_2L conformers were investigated in the gas-phase and methanol using B3LYP/6-311++G** level of theory. The optimized geometries and minimum energies of all conformers were registered in **Table 1.** The six conformers of H_2L were sorted out in descending order starting from E-cis with the lowest energy hence being the most stable conformer. It is thus considered the reference substrate. It is immediately followed by E-trans. The energy difference between these two conformers is negligible (0.13 kcal/mol). Therefore, they could be considered existing as a stable mixture. The H_2L ligand could lead to a number of isomers and tautomers. Its isomers result from the rotation around single bonds, e.g. E-cis and E-trans; while the tautomers originate from the difference in functional groups e.g. E-cis and K-cis. Additionally, the relative energies indicate that the energy difference between the most stable di-keto (KK) and di-enol (EE) forms is 9.90 kcal/mol. This amount of energy is certainly sufficient for a proton transfer between these tautomers at room temperature. Moreover, the excited state E-cis* (-1149.9166 a.u.) is lower in energy compared to the K-cis* (-1149.8962 a.u.) tautomer. This means that E-cis is the most stable species in the excited state as well. Here again, this is the second reason for

the E-cis to be considered as the reference substrate. This finding provides an early clue for the fact that the E-cis does not follow the ESIPT mechanism.

The effect of methanol on the structures of these H_2L ligands is investigated using B3LYP/6-311++G** level of theory. The solvation results were completely in line with those in the gas-phase. The E-cis ligand in methanol is more stable than in the gas-phase and still the most stable species.

Table 1: The optimized structures and minimum energies of H_2L ligand conformers in gas-phase and methanol obtaining by using B3LYP/6-311++G** level of theory.

Conformers	Structure	Relative Energy (kcal/mol)	
		Gas Phase	Methanol
E-cis	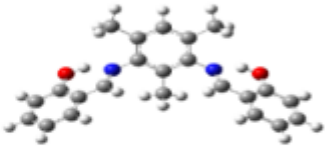	0	0
E-cis*		33.82	57.85
E-trans	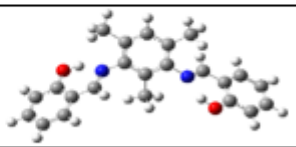	0.12	0.37
EK-trans	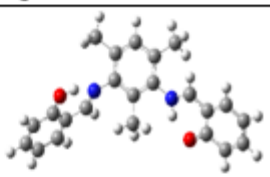	4.7	1.94
K-cis	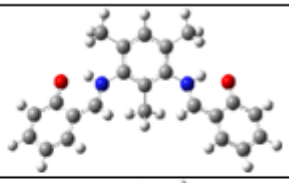	9.91	3.95
K-Cis*		46.62	45.93
K-trans	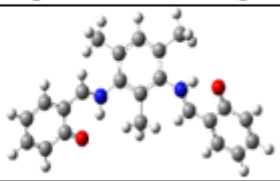	9.91	4.20
K-Cis-2	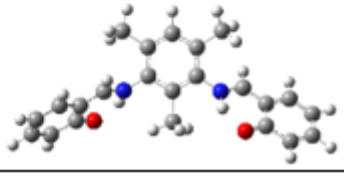	10.91	4.83

3.2 Protonation and Deprotonation

The studied compounds possess two positions which can accept protons and one site which can donate a proton. The literature seems to lack a systematic study of the electronic structure, bonding characteristics and acid–base properties of this class of compounds. FT calculations were employed to

investigate sites of protonation of these compounds. Furthermore, the acid-base properties of ligands in **Table S1** will be examined and theoretical proton affinities and deprotonation enthalpies will be computed. Nevertheless, since most protonation processes occur in solution, so the characteristics of the protonation and deprotonation will vary with the properties of the solvent used.

All the possibilities of the protonation/deprotonation of E-cis are investigated. **Table S1** displays geometry optimized structures and minimum energies of the protonation/deprotonation forms in the gas-phase and in methanol as a solvent. On the one hand, in the first protonation process, the proton is added exergonically to a one nitrogen atom, yielding (H_3L^+) with an energy difference of 240.587 and 275.539 kcal/mol compared to that of the parent ligand (H_2L), in the gas-phase and methanol, respectively. On the other hand, the reverse deprotonation process, where the proton is extracted endergonically from an oxygen atom producing (HL^-), requiring an energy difference of 325.153 and 306.852 kcal/mol compared to those of the parent H_2L ligand, in the gas-phase and methanol, respectively. Likewise, in the second protonation process, the proton is added exergonically to the other nitrogen atom generating (H_4L^{+2}), with an energy difference of 429.782 and 547.377 kcal/mol compared to those of the H_2L ligand in gas-phase and methanol, respectively. Conversely, the reverse second deprotonation process, where the second proton is extracted endergonically from the other oxygen atom creating (L^{-2}), needed an energy difference of 750.439 and 615.901 kcal/mol compared to those of the neutral ligand (H_2L) in the gas-phase and methanol, respectively. In a nutshell, we could conclude easily that the protonation process of E-cis tautomer is energetically extremely favorable, while its deprotonation process seems to be considerably unfavorable energetically.

3.3 Absorption and Emission Spectra (UV-Vis) of Ligands

Starting from the optimized ground state geometries, we investigated the absorptions to the vertical singlet excited states by using different TDDFT functionals namely: B3LYP, CAM-B3LYP, M06-2X and ωB97X with the 6-311++G** basis set. In **Figure S1**, the simulations of UV-Vis spectra of the E-cis tautomer are shown, where (a) displays the electronic transitions using the optimized structure coming from the B3LYP/6-311++G** level of theory and (b) displays the electronic transitions applying the optimized structure coming from the different functionals. Furthermore, the details of the excitation energies and oscillator strengths, as well as the excited state compositions for the E-cis tautomer are reported in **Table S2**. Experimentally, the electronic absorption spectrum of the E-cis tautomer shows intense bands at 314 and 258 nm corresponding to the n→π* and π→π* transitions, respectively. It is clear that the B3LYP functional transition signal (H→L at a wavelength of 314.5 nm and an oscillator strength of 0.033) is comparatively in excellent agreement with the experimental results [1]. It produced another stronger (oscillator strengths of 0.148) electronic transition (H-4→L) at 257.5 nm which is approximately superimposed on its experimental peer. As for the other DFT functionals, their agreement with the experimental counterparts ordering is as follows: M06-2X > CAM-B3LYP > ωB97XD. As listed in **Table S2**, we observed generally that the values of column (b) obtained from these three functionals are close to the experimental values [1]. Additionally, the transition signals obtained from CAM-B3LYP

functional in columns (a) and (b) are 312.943 and 304.056 nm, respectively; while their peers from M06-2X are 251.521 and 265.737 nm, respectively. Comparatively the ωB97XD signals divert far from the experimental ones [1]. These findings support the adoption of the B3LYP functional in subsequent calculations.

Figure 2 depicts the UV-Vis spectra of E-cis in the gas-phase and methanol obtained by using TDDFT/B3LYP/6-311++G** level of theory. The effect of using methanol as a solvent on the values of the calculated electronic $n \rightarrow \prod^*$ transition yielded only a difference of *ca.* 3.5 nm compared to that of the gas-phase. In contrast, the electronic transition $\prod \rightarrow \prod^*$ transition has a wavelength maximum nearly superimposable on both the experimental [1] and gas-phase values. Generally, the high values of the oscillator strengths obtained when methanol is used as a solvent, indicate more absorption efficiency in solution compared to that in gas-phase.

Table 2 shows the visualization of the Natural Transition Orbitals (NTO) of E-cis tautomer in the gas-phase and methanol as a solvent obtained by using TDDFT/B3LYP/6-311++G** level of theory. Here the hole represents the space that the electron leaves in HOMOs due to the electronic excitation. In contrast, the particle represents the space the electron occupies in LUMOs due to the electronic excitation.

Table 2: *Natural transition orbitals visualization of E-cis in the gas phase and methanol as a solvent obtained by using TDDFT/B3LYP/6-311++G** level of theory*

Gas Phase		Methanol	
Hole	**Particle**	**hole**	**particle**
(λ = 314.467 nm) n⟶ **π***		(λ = 317.967 nm) n⟶ π*	
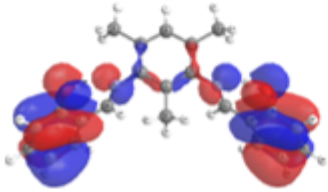	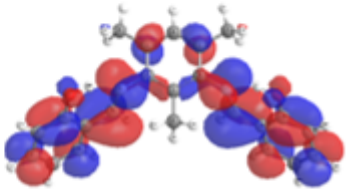	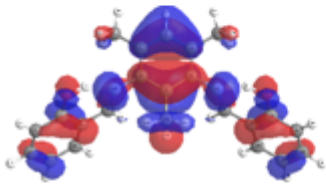	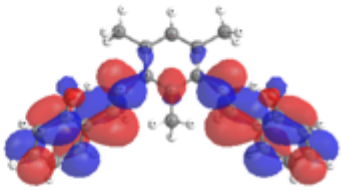
(λ = 257.460 nm) **π ⟶ π***		(λ = 258.210 nm) π ⟶ π*	
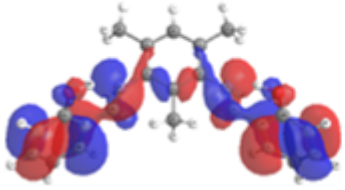	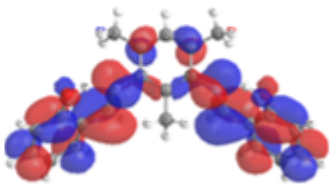	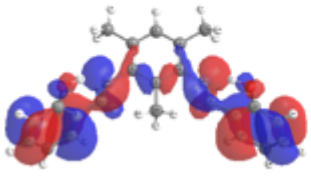	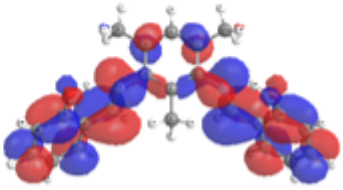

The estimation of energy gaps is quite important, especially for the electronic excitation analysis, because the value of the energy gap is taken as an indication of the probability of the fluorescence emission.

Table 3 *registers the HOMO, LUMO and Energy Gaps values of the various H_2L conformers obtained by using B3LYP/6-311++G** level of theory. We notice here that the E-cis and E-trans tautomers have the*

highest energy gaps values. This does not mean that they have the most potent fluorescence emission, but it supports our conclusion for selecting both E-cis and E-trans as the most stable mixtures with the lowest energy.

Table 3: *The calculated HOMO, LUMO and Energy Gap of the various H_2L ligand forms obtained by using B3LYP/6-311++G** level of theory.*

Ligand Form	HOMO (eV)	LUMO (eV)	Energy Gap (eV)
E-cis	-6.023	-1.959	4.064
E-trans	-6.054	-1.959	4.095
EK	-5.637	-2.17	3.467
K-cis	-5.772	-2.384	3.388
K-trans	-5.733	-2.35	3.383
K-cis-2	-5.756	-2.324	3.432

*To simulate the emission UV-Vis spectra of the E-cis tautomer in gas-phase and methanol; we used TDDFT/B3LYP/6-311++G** level of theory on their optimized structures obtained by using B3LYP/6-311++G** level of theory.* ***Table 4*** *lists the electronic emission energies and oscillator strengths as well as the ground state compositions of the E-Cis tautomer. Experimentally, the electronic emission spectrum of the E-Cis tautomer doesn't show any noticeable fluorescence upon excitation at 350 nm. However, at 458 nm some of the H_2L metal complexes showed intense fluorescence band. The gas-phase π*→n emission transitions which were assigned to L→ H and L+1→ H movements that gave the wavelengths 451.560 and 440.318 nm (2.746 and 2.816 eV with 0.55 and 0.49 %), respectively, had zero oscillator strengths. On the contrary, the positive effect of using methanol as a solvent is manifested in raising the fluorescence efficiency. Here the π*→n emission signals are assigned to L→ H and L+1→ H transitions; which gave rise to the wavelengths 497.631 and 455.475 nm (2.491 and 2.722 eV; both 0.69%) with 0.083 and 0.107 oscillator strengths, respectively.*

Table 4: *Electronic emission energy, corresponding oscillator strengths and the corresponding MO compositions of E-cis tautomer in the gas-phase and methanol obtained by using TDDFT/B3LYP/6-311++G** level of theory. (Exp. 458 nm; Ref.1).*

E-cis	$\lambda_{(nm)}$	E_{ex} (eV)	ƒ	Composition	Coefficient
Gas-Phase	451.560 440.318	2.746 2.816	0.000 0.000	H→L H→L+1	0.55 0.49
Solvent (Methanol)	497.631 455.475	2.491 2.722	0.083 0.107	H→L H→L+1	0.69 0.69

Table S2 *shows the NTO visualization of E-Cis tautomer emission in the gas-phase and methanol which were obtained by using TDDFT/B3LYP/6-311++G** level of theory. The electron excitation has changed the ground state optimized structure of E-cis tautomer. These variations were observed through the change of some bond types (from single to double bond and vice versa) and the bond angles. That is to say, an electron transfer occurs after the photoexcitation, called Photo-induced Electron Transfer (PET) mechanism.*

Figure 3 *shows the geometric changes on one side of E-cis tautomer. It is clear that both C1–C2 and C3-N21 bonds are shortened by ca. 0.02 and 0.09Å, respectively, due to the formation double bonds. On the other hand, the N21-C23 bond is lengthened by 0.14Å, as a result of the formation of a single bond. Simultaneously, the bond angle δ(C3–N21–C23) opened up by 4°. To understand the PET mechanism, we consider the central aromatic group namely the 2,4,6-trimethyl benzene (TMB) as an acceptor and the azomethine group (AZM) as a free donor. Upon the photoexcitation, an electron is excited from a π-type bonding molecular orbital to the π*-type antibonding molecular orbital i.e. this transition corresponds to the transition from the HOMO-n orbital (any orbital of π-type) of AZM to the LUMO orbital of TMB. Simultaneously, the lone pair on the N21 of AZM as a HOMO orbital with higher energy than the HOMO-n orbitals allows one of the electrons of the lone pair to transfer from the HOMO orbital to a HOMO-n orbital. This process prevents the excited electron from returning to the HOMO-n orbital, which leads to a fluorescence quenching [38]. Methanol relatively reduces the effect of the PET process through the formation of a hydrogen bond between the N21 of the AZM and the hydrogen atom of the hydroxyl group of the methanol.*

3.4 Excited State Intramolecular Proton Transfer (ESIPT)

For investigating the ESIPT mechanism using H_2L ligands, we compared the structural changes around the proton to be transferred in both the ground and excited states. Table **S3** shows these structural changes for both the gas-phase and methanol-solvated E-cis and K-cis tautomers. It clears that the O47–H48 bond is shortened by 0.003 Å, while the H48–N20 bond is lengthened by 0.016 Å in going from the ground state (S_0) to the excited state (S_1) of both the gas-phase and methanol-solvated E-cis tautomer. Furthermore, the O47–H4-N20 bond angles are hardly changeable by photoexcitation in both phases. The small increase of the O47-H48 bond and the negligible decrease of bond angle δ(O47–H48-N20) demonstrate the formation of a relatively weaker hydrogen bond in the excited state (S_1). These structural changes oppose the concept of ESIPT process from the E-cis tautomer. Comparatively for the K-cis configuration, it is noted that the O4-H48 bond is increased by 0.014 and 0.006Å in the excited (S_1) state in the gas-phase and methanol, respectively; while the H48–N20 bond length is decreased by 0.002 and 0.001 Å on excitation in the gas-phase and methanol, respectively. Simultaneously, the bond angles δ(N20–H48-O47) were hardly changed in both the gas-phase and methanol. These changes indicate that the possibility of proton transfer from E-cis to K-cis occurs only in the ground state (S_0) and the photoexcitation does not cause a proton to transfer in the first excited state (S_1) [40]. We shall support

these results by studying the potential energy curve which shows a proton transition between E-cis and K-cis tautomers in the ground state.

3.5 Study of Complexes

3.5.1 Geometry and Binding Energies of Complexes

An interaction between the parent ligand ion (L^{2-}) and Zn^{2+} ions to form complex **(1)** with an L:M ratio of 2:2, as reported experimentally in literature [1], is theoretically investigated as a fluorescence probe as well as a molecular-switching device. After optimization of both L^{2-} and complex $[Zn_2L_2]$ **(Complex 1)**, the interactions of the latter with Ag^+ and Cu^{2+} ions forming complexes $[Zn_2L_2].[Ag^+]_2$ and $[Zn_2L_2].[Cu^{2+}]^2$ hereafter, named **Complex 7** and **Complex 9**, respectively, are studied. For open-shell species, the unrestricted orbitals were employed, and high-spin complexes were considered, that is, the spin multiplicities considered were 1 and 3 for Cu2+ complexes resulting in **Complex 9S** and **Complex 9T**, respectively. The different geometric structures of all the studied complexes of Zn^{2+}, Cu^{2+} and Ag^+ are listed in **Table S4.** They were obtained by using B3LYP/LANL2DZ/6-311++G** level of theory. Their binding energies in both the gas-phase and methanol were estimated using the aforementioned level of theory and registered in **Table S4**.

The first seven binuclear complexes are formed by the conjugation of two L^{2-} ions with two metal ions (L:M, 2:2), where the filled four lone pairs on two nitrogen atoms (-CH=N-) and two oxygen atoms ($-O^-$) interact with the four empty sp^3 molecular orbitals of the metal ions to form distorted tetrahedral shapes. The objective of the present work is to investigate effect of Cu2+ and Ag^+ ions on the electronic structure, absorption and emission spectra of **Complex 1.** Upon the binding of two Cu2+ or two Ag^+ metal ions with **Complex 1**; one ion chelates with two oxygen atoms of the ligand and the other one formed cation-π interaction with the benzene rings with an M:L:M ratio of 2:2:2 as shown in **Table 6**. It is also noticeable from the optimized structures of the two complexes of **1**-$2Cu^{2+}$ (**Complex 9**) and **1**-$2Ag^+$ (**Complex 7**) that one ion is up and the other is down.

For more understanding of the metal-ligand complexation, it is better to recall that the Zn2+, Cu2+ and Ag^+ electron configurations are: $[Ar]3d^{10}\ 4s^0\ 4p^0$, $[Ar]\ 3d^9\ 4s^0\ 4p^0$, $[Kr]\ 4d^{10}\ 5s^0\ 5p^0$, respectively. The empty s- and p-type orbitals are hybridized to form four empty sp^3 orbitals with equal energies. They have the ability to form covalent coordination bonds with the four lone pairs of the L^{2-} ions.

The experimental and theoretical values of the bond lengths of complexes **(1)** and (**2T**) are collected in **Table S5** for comparison. In the case of the complex **1** ($[Zn_2L_2]$), the four nitrogen atoms form a symmetric ligand L^{2-} metal ion substrate with distances of 2.081 Å and 2.091 Å for [Zn-N1] and [Zn-N2], respectively; while the four oxygen atoms reach distances of 1.980 Å, and 1.982 Å for [Zn-O1] and [Zn-O2], respectively, making up a distorted tetrahedral geometry (Td) about the metal centers with Zn-Zn separation of 6.722 Å. These findings are in good agreements with the experimental single crystal

structure of this complex [1]. The Zn-N and Zn-O distances in a methanol-solvated complex **1** are slightly elongated with [Zn-N1] of 2.134 Å, [Zn-N2] of 2.032 Å, [Zn-O1] of 2.031 Å, and [Zn-O1] 2.032Å. These deviations explain the decreasing stability of complex **1** in methanol compared with its structure in the gas-phase.

The bond lengths of Cu-O and Cu-N in $[Cu_2L_2]$. H_2O complex range between 1.972 -1.947 Å and 2.051-2.065 Å, respectively. These range values agreed favorably with the expected range observed for copper complexes [41] and the values reported in X-ray analysis [1] for this particular complex. The crystal structure of **2** displayed the existence of one water molecule in lattice. DFT calculation indicated that the H_2O molecule forms hydrogen bonds which increased the stability of the complex.

In this work, we focus, primarily, on the interaction between L^{2-} ligands and Zn^{2+} ions leading to Complex **1**. We then investigate the interaction of complex **1** with Ag^+ and Cu^{2+} ions yielding different complexes that might be of importance. The binding energies are calculated for all the studied complexes in both the gas-phase, methanol and water as a solvent. The results are listed in **Table 6**. It is clear from the results that the binding energies in the gas-phase were generally more negative than those in the solvent. This is because the solvent molecules prevent effective interactions between the ligands and metal ions. The binding between the ligand and metal ions in water were generally more effective than in methanol. This is because the former allows the formation of hydrogen bonds in these complexes.

According to the binding energy values, the order of the stability of the complexes in the gas-phase is as follows: **9T**>**9S**>**8D** >**8U** >**7**>**2T**>**2S** >**3**>**4**>**6**>**1**>**5**. The formation of Cu2+ 2S complex requires more energy for pairing the unpaired electrons leading to diamagnetic properties. This is manifested through the amount of the binding energy of -1.521 a.u. for **2S** and -1.572 a.u. for **2T** where the pairing energy is unrequired for the latter Accordingly, we can adopt **2T** as a reference, because it contains the unpaired electrons, that earn **2T** the high spin and the paramagnetic properties that might affect, later on, the electronic emission process. In addition, the complexes that are formed through weak interactions between complex **1** and Ag^+ ions ($[Zn_2L_2].[Ag^+]_2$ **(7)**) or Cu2+ ions ($[Zn_2L_2]$.[Cu2+], where the Cu2+ ion is down (**8D**)) or ($[Zn_2L_2]$.[Cu2+], where the Cu2+ ion is up (**8U**)); the binding energies in the gas-phase render their order of stability as follows: **8D** > **8U** > **7**, with a slight difference between **8U** and **8D** of *ca.* 0.015a.u. On other hand, the strongest complexes are formed when two Cu2+ ions chelate in singlet (**9S**) or triplet (**9T**) states with complex **1**, where one Cu2+ ion interacts at the top through cation-π bonding and the other one at the bottom through oxygen atoms lone pairs. Finally, our theoretical study showed that **8D** is the most stable complex, complementing the fact that has been isolated and identified experimentally [1].

The Cu2+ and Ag^+ ions are bonded to complex **1** through the cation-π interaction between trimethy benzene (TMB) rings or/and through the weak interaction with the lower two oxygen atoms lone pairs. The energies of HOMOs, LUMOs and Energy Gaps are listed in **Table S6**.

The Ag^+ ions are considered electron acceptors due to the presence of four empty sp^3-hybridized orbitals, where the interaction with complex **(1)** causes the charge transfer towards the silver ions. The results listed in **Table S5** indicate that the energy gap of complex **1**-2Ag^+ is quite close to that of complex **1**. These results explain why Ag^+ ions keep enhancing the fluorescence bands [1].

On other hand, the Cu2+ ion is considered an electron donor due to the presence of the unpaired electron in the t_{2g}^5 degenearte orbitals, which interact with complex **1** through charge transfer towards the TMB rings and/or towards the lower two oxygen atoms. In case of the complexes **8D** and **8U**, this charge transfer results in an increase of the energy gap and hence subsequent blue shift effects on the absorption and emission spectra leading to fluorescence enhancement. In contrast, Complex **9S** , a low spin Cu2+-complex **(1)** adduct with a chemical formula $[Zn_2L_2]\cdot[Cu2+]_2$, shows a severe decrease in the energy gap (0.312 eV) that causes fluorescence quenching. This latter complex is different from the copper complex reported in literature [1] {$[Zn_2L_2]\cdot[Cu2+]$ }. In conclusion, the ICT mechanism confirms that complex **1** acts as a fluorescent Photoionized Charge Transfer (PCT) sensor for Ag^+ or Cu2+ ions [1].

3.5.2 Absorption and Emission Spectra (UV-Vis) of Complexes

B3LYP, CAM-B3LYP, M06-2X and ωB97X functionals with a mixed basis set LANL2DZ/6-311++G** were applied to investigate the absorptions to the vertical singlet excited states. Details of the excitation energies and oscillator strengths, as well as the excited state molecular orbital compositions for complex **1**, are reported in **Table 7.** Experimentally, the electronic absorption spectrum of complex **1** displays intense bands at 398 and 278nm corresponding to n→π* and π→π* transitions, respectively [1]. TDDFT results indicate that the B3LYP functional signals were comparatively in excellent agreement with the experimental results [1]. The B3LYP functional gives H→L+1 electronic transition at a wavelength of 396.36nm (3.13 eV) and an oscillator strength of 0.099 with a percentage of 48%. The other H-2→L+4 electronic transition gives a wavelength of 275.56nm (4.499 eV) and an oscillator strength of 0.012 with a percentage of 53%. Concerning the other functionals, the ordering according to their agreement with the experimental results is as follows: M06-2X > CAM-B3LYP > ωB97XD. In particular, the M06-2X functional gives a signal at 278.261nm (4.456 eV) with an oscillator strength of 0.018 with a percentage of 50% due to the electronic transition H-3→L; in addition to a π→π* electronic transition with a wavelength value in very close agreement with the experimental value [1].

Table 5: *Electronic absorption energy (nm/eV), corresponding oscillator strengths and assignments of $[Zn_2L_2]^0$ obtained by using various TDDFT functionals with mixed LANL2DZ/6-311++G** basis set (Exp. (nm): 398 and 278 Ref.1)*

Functional	$\lambda_{(nm)}$	E_{ex} (eV)	f	Assignment	Coefficient
B3LYP	396.358	3.128	0.099	H→L+1	0.48
	368.794	3.362	0.142	H-2→L+1	0.49
	277.520	4.468	0.000	H→L+4	0.68
	275.559	4.499	0.012	H-1→L+4	0.53
CAM-B3LYP	357.625	3.467	0.047	H-1→L+3	0.51
	350.230	3.540	0.548	H-1→L+2	0.52
	273.299	4.537	0.059	H-2→L	0.52
	248.089	4.998	0.049	H-1→L	0.46
M06-2X	351.481	3.527	0.560	H-1→L+2	0.51
	344.891	3.595	0.120	H-2→L+2	0.56
	278.261	4.456	0.018	H-3→L	0.50
	244.797	5.065	0.188	H-9→L+1	0.36
ωB97XD	356.678	3.476	0.045	H→L+3	0.51
	343.239	3.612	0.117	H→L+2	0.54
	260.325	4.763	0.208	H-2→L	0.40
	179.738	6.898	0.200	H-1→L+7	0.41

Details of the excitation energies and oscillator strengths, as well as their assignments and coefficients for E-cis ligand and complexes **(1), (2S), (2T), (7), (8U), and (8D)** are reported in **Table S6.** Experimentally, the electronic absorption spectra of these complexes display intense bands due to the n→π* and π→π* transitions. The weak absorptions of the complexes **(2T)**, **(8D)** and **(8U)** are observed in the UV range (340-440nm), whereas the compounds E-cis**, (1), (2S)** and **(7)** show strong absorption bands in the range between 240 and 300nm. The π→π* electronic transitions of the complexes show red shifts compared to those of the E-cis ligand in excellent agreement with measured values [1]. Furthermore, complex **2T** displayed the H-5α→L+1α electronic transition with a maximum wavelength at 326.585nm (3.796 eV) an oscillator strength of 0.005 with a percentage of 45%, that nearly approximates that of complex **2S** and the experimental value [1]**.** In addition, complex **8D** exhibited maximum wavelength quite close to that of the experimental value compared to that of **8T**. In general, the weak absorptions in complexes **(2S), (2T), (2D) and (2T)** visible spectra indicate their poor efficacy in exhibiting fluorescence. **Figure 5** depcits the simulated absorption spectra of complexes **1, 7** and **8D** for verifying the effect of the ICT mechanism. The p®p* electronic transition of complex **1** is red shifted (from 269 to 290 nm) in complex **7**; while its n®p* transition is blue shifted (from 368 to 330 nm) in complex **8D.** It is clear that the redshift

effect is more pronounced than the blueshift impact. This is because the energy gap difference between complexes **1** and **7** (*ca.* 1.072 eV) is greater than the that between complexes **1** and **8D** (*ca.* 0.117 eV).

The studied lignad-metal complexes contain six benzene rings in addition to four oxygen and four nitrogen atoms. This chemical composition results in many n®p* and p®p* elctronic transitions. The natural transition orbital (NTO) visualizations depicted in **Table S8** display the origin (hole) and destination (particle) of the electron of complexes **1, 7** and **8D** upon the photoexcitation in both gas-phase and methanol using TDDFT/B3LYP/LANL2DZ/6-311++G** level of theory. It is clear from **Table 6** that the values of the energy gaps of the E-cis ligand and its complexes in different functionals are different upon the photoexcitation. It is interesting to note that the energy gaps estimated by B3LYP, CAM-B3LYP, M06-2X and ωB97XD functionals for complex **2T** compared to those of complex **1,** are decreasing from 3.587, 6.062, 5.666 and 7.22 to 2.186, 4.74, 5.024 and 5.866 eV, respectively. On the other hand, the comparison of the energy gaps for complexes **7** and **8D** using the same functionals are increasing from 0.331, 1.067, 0.816 and 2.166 eV to 2.495, 4.927, 4.536 and 6.155 eV, respectively. It is noteworthy that the energy gap values after photoexcitation give an initial impression of the occurrence of explicit fluorescence of the target compounds when compared to each other. This conjecture is clear in **Figure 6** where a larger energy gap value of complex **7** indicated fluorescence enhancement and a lower energy gap value in complex **8D** marked fluorescence quenching [1].

Table 6: *Electronic emission energy (nm/eV), oscillator strengths (f), assignment of MOs and their coefficients for E-cis (6-311++G**) and its complexes in methanol obtained by using TDDFT/B3LYP functional with 6-311++G** and LANL2DZ/6-311++G** basis sets. (Exp. 458 nm Ref.1).*

Compound	λ (nm)	$E_{ex.}$(eV)	F	Assignment	Coefficient
E-cis	497.631	2.49	0.08	L→H	0.69
	455.475	2.72	0.107	L+1→H	0.69
1	451.429	2.747	0.130	L→H-1	0.60
	411.009	3.017	0.032	L+2→H	0.62
	385.381	3.217	0.232	L+2→H-1	0.66
7	406.881	3.047	0.048	Hα→Lα	0.60
	385.274	3.218	0.485	L+2α→Hα	0.53
8D	496.277	2.498	0.000	L+3β→H-2β	0.48

The emission light produced from the deactivation of the excited states as an opposite action of the absorption process is relatively time consuming. Moreover, the normal termination of the emission calculations for the complexes that quenched the fluorescence was extremely difficult and tricky. In ***Figure 7*** *is depicted the emission spectrum of complex* ***1*** *in both the gas-phase and solution (methanol) obtained by using TDDFT/B3LYP/ LANL2DZ/6-311++G** level of theory together with its experimental one for comparison purposes. It is noteworthy that the emission spectrum using methanol (451.43nm) is in excellent agreement with the experimental (458nm) one besides it is extremely intense; while that simulated in the gas-phase is relatively weak and diverges by ca. 57nm form the observed value [1]. The*

*simulated and experimental emission spectra of E-cis ligand and complexes **1**, **7** and **8D** in methanol are pictured in **Figure 8.** It is clear that both E-cis ligand and complex **8D** have extremely weak emission signals in excellent agreement with experiment [1]; while the theoretical and experimental emission spectra of complexes **1** and **7** are comparatively very intense and close to each other. It is interesting to note that the intensity of simulated emission spectrum of complex **7** is greater than that of complex **1** confirming the fluorescence enhancement on the addition of Ag^{+} ions [1]. On the contrary, the extremely small intensity of the simulated emission spectrum of complex **8D** as a result of adding the Cu2+ ions to complex **1** could be explained in terms of fluorescence quenching [1]. The order of the simulated intensity of fluorescence for these substrates is as follows: **7** > **1** > **8D** ≈ E-cis in excellent agreement with experiment [1].*

***Table 7** registers the details of the electronic emission energies, oscillator strengths as well as the assignments and coefficients of MOs for E-cis and complexes **1**, **7** and **8D** in the methanol as a solvent. The p*®p electronic emission transition of E-cis ligand (L+1→H) showed a very weak band (**f**=0.107) at 455.475nm with a deviation of ca. 2.5nm. The π*→n emission electronic transition of E-cis (L→H) and complex 8**D** (L+3→H-2) showed very weak bands at 497.6 and 496.2nm, respectively. The oscillator strength of complex **8D** is zero indicating fluorescence quenching on the addition of Cu2+ to complex **1**. Conversely, the p*®p electronic emission transition of complexes **1** (L+2→H-1) and **7** (L+2α→Hα) exhibited very intense bands both around 385nm. They acquire oscillator strengths of 0.232 and 0.485, respectively; which indicated the fluorescence enhancement by the Ag^{+} ion chelation to complex **1**. Moreover, we observed the π*→n emission transitions of complexes **1** (L+2→ H) and **7** (Lα→Hα) that yielded wavelengths at 411.01 and 406.88nm and oscillator strengths of 0.032 and 0.048, respectively. Here, too, the fluorescence intensity improves clearly in complex **7** through the interaction of silver ions with complex **1**; which squarely agreed with experiment [1].*

As we previously mentioned, both L^{2-} ligand and its complexes contain six benzene rings in addition to four oxygen and four nitrogen atoms; a situation that renders the electronic structure of these substrates full of p®π and p*®n transitions. In **Table 8** are exhibited the positions of origin and destination of the excited electron in complexes **1**, **7** and **8D** upon the photoexcitation which results in the fluorescence emission. In fact, since the fluorescence of complex **1** arises from an irreversible reaction between E-cis and the Zn^{2+} ions, then E-cis can be classified as a fluorescent probe of a chemodosimeter type [2]. On the other hand, the fluorescence of complex **1** is enhanced or quenched by a reversible reaction with Ag^{+} or Cu^{2+} ions, respectively. These actions render complex **1** as a fluorescent probe of a chemosensor type [41].*

***Table 7:** Natural transition orbitals (NTO) visualization of ligand and its complexes in methanol estimated by using TDDFT/B3LYP/ LANL2DZ /6-311++G** level of theory.*

Complex	Particle	Hole
1	(λ =411.009 nm) π* ⟶ n	
	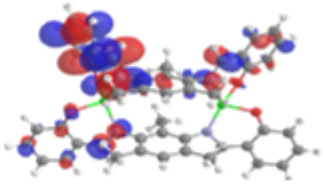	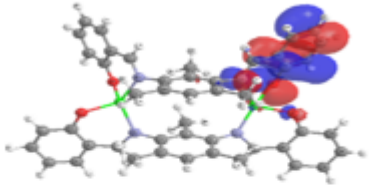
7	(λ =406.881 nm) π* ⟶ n	
	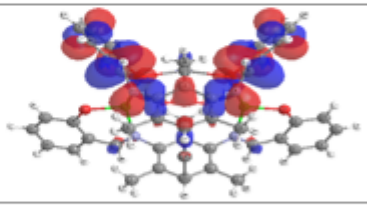	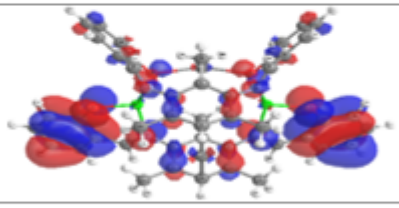
8D	(λ = 496.277 nm) π* ⟶ n	
	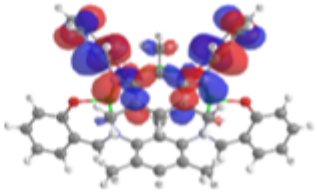	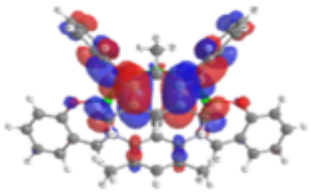

3.6 Effect of Metal Ion Chelation

*The E-cis is a chelating ligand that interacts irreversibly with metal ions leading to different actions like enhancing or quenching fluorescence depending on the nature of the metal ions. The chelation of the deprotonated form of E-cis (L^{2-}) with Zn^{2+} ions reduces the energy of the HOMO orbital formed of the lone pair of N21 of the azo moiety of the ligand. Thus, the electron excited from HOMO to LUMO of the TMB returns to the HOMO, thus inhibiting the PET process and restoring fluorescence. This is called a chelation enhanced fluorescence (CHEF) effect [42]. On other hand, the chelation of the Cu^{2+} ion leads to the inhibition of the PET process like the previous mechanism but quenches the fluorescence; called chelation quenched fluorescence [43]. This action could be attributed to high spin and paramagnetic behaviour of complex **2T**. **Figure 9** illustrates a general summary of the most important substrates and the ultimate results obtained in the present work.*

4. Conclusion

This work aims to investigate the reasons that lead to the difference in the intensity of fluorescent behavior of the molecular designs that allows to detect Zn^{2+}, Cu^{2+}, and Ag^{+} metal ions using a computational study.

The geometry optimization has been performed using B3LYP functional which was adopted as the best functional for the absorption and emission calculations. The use of methanol as a solvent proved useful in the DFT and TDDFT methods.

The E-cis isomer is the most stable conformer with a rotation barrier of 0.12 kcal/mol to give the E-trans counterpart. On the other hand, it is the most stable tautomer with a potential energy barrier of 6.65 kcal/mol to give the K-cis tautomer in the ground state only, a fact that could deny the occurrence of ESIPT mechanism. Fluorescence quenching of E-cis through the occurrence of a PET mechanism was evidenced by the change in the electronic structure.

The irreversible interaction between E-cis and the Zn^{2+} ion leads to the inhibition of the PET process and enhances fluorescence by the CHEF effect. Thus, the E-cis isomer could be adopted as a fluorescent probe (type a chemodosimeter) for Zn^{2+} ion. While the irreversible interaction between E-cis and the Cu^{2+} ion leads to inhibiting the PET process and quenching of fluorescence by the CHQF effect. This could be attributed to the high spin and paramagnetic arrangement of complex **2T**. This means that E-cis is not a fluorescent probe for Cu^{2+} ion.

The reversible interaction between complex **1** and the Ag^{+} ion (electron acceptor) leads to the enhancement of fluorescence through the ICT mechanism. This is achieved by a decrease in the energy gap, which leads to the redshift of the absorption spectrum. Thus complex **(1)** behaves as a fluorescent probe of type a chemosensor *i.e.* a fluorescent PCT sensor for the Ag^{+} ion. Additionally, the reversible interaction between complex **1** and the Cu^{2+} ion (electron donor) leads to the quenching of fluorescence through the ICT mechanism. It originates from an increase of the energy gap value, which leads to the blueshift of the absorption spectrum. Thus complex **1** could function as a fluorescent probe of type a chemosensor or, specifically, a fluorescent PCT sensor for Cu^{2+} ion.

Finally, we conclude that complex **1** could act as an “On-Off-On” molecular switch by exchanging Cu^{2+} and Ag^{+} ions. This finding is in excellent agreement with the experimental study.

Declarations

Acknowledgement

The authors acknowledge with thanks the technical support and funding by the Deanship of Scientific Research (DSR), King Abdulaziz University, Jeddah, under grant no. 140-130-1440. The authors are also grateful to the HPCC (Aziz Supercomputer) for the resources.

Author’s Declarations

Funding- by the Deanship of Scientific Research (DSR), King Abdulaziz University, Jeddah, under grant no. 140-130-1440.

Conflicts of interest/Competing interests- Not Applicable

Ethics approval/declarations- Not Applicable

Consent to participate- Not Applicable

Consent for publication- Not Applicable

Availability of data and material/ Data availability- The datasets generated during the current study are available from the corresponding author on reasonable request.

Code availability- Not Applicable

Authors' contributions- Shaaban Elroby, Osman I Osman and Bashair Abdullah Banaser conceived, designed, performed the calculations enriched the research point, conducted the theoretical calculations and did the writing up of the manuscript; Abdesslem Jedidi and Walid I Hassan surveyed the literature and facilitated the research work; Saad Aziz helped with lab facilities and critical revision of the manuscript. All authors shared equally the revision of the final version.

References

1. Pandey, R. et al. Fluorescent zinc(II) complex exhibiting 'on-off-on' switching toward Cu2+ and Ag+ ions. Inorg. Chem. 50, 3189–3197 (2011).
2. Sedgwick, A. C., Wu, L., Han, H. H., Bull, S. D., He, X. P., James, T. D., Sessler, J. L., Tang, B. Z., Tian, H., & Yoon, J. (2018). Excited-state intramolecular proton-transfer (ESIPT) based fluorescence sensors and imaging agents. *Chemical Society Reviews*, *47*(23), 8842-8880.
3. Mahal, A. et al. Synthesis, Characterization and Antifungal Activity of Some Metal Complexes Derived From Quinoxaloylhydrazone. 3, 1–8 (2015).
4. a) C. M. Metzler, A. Cahill, D. E. Metzler, J. Am. Chem. Soc. 1980, 102, 6075; b) A. Adabiardakani, M. Hakimi, H. Kargar, World Appl Programming 2012, 2, 472.
5. a) A. Kajal, S. Bala, S. Kamboj, N. Sharma, V. Saini, J. Catal. 2013, 2013, 1; b) A. Jarrahpour, D. Khalili, E. De Clercq, C. Salmi, J. M. Brunel, Molecules 2007, 12, 1720.
6. Y. Elerman, M. Kabak, A. Elmali, Z. Naturforsch. B 57 (2002) 651.
7. M.M.H. Khalil, M.M. Aboaly, R.M. Ramadan, Spectrochim. Acta (Part) 61 (2005)157.
8. N. Chantarasiri, V. Ruangpornvisuti, N. Muangsin, H. Detsen, T. Mananunsap, C.Batiya, N. Chaichit, J. Mol. Struct. 701 (2004) 93.
9. A.A. Soliman, G.G. Mohamed, J. Thermochim. Acta 421 (2004) 151.
10. Feringa, B. L., Browne, W. R., Eds. Molecular Switches: Second, Completely Revised and Enlarged Edition; Wiley-VCH, Weinheim, 2011.
11. Ogawa, K.; Kasahara, Y.; Ohtani, Y.; Harada, J. Crystal Structure Change for the Thermochromy of N-Salicylideneanilines. The First Observation by X-ray Diffraction. J. Am. Chem. Soc. 1998, 120, 7107-7108
12. Hadjoudis, E.; Mavridis, I. M. Photochromism and Thermochromism of Schiff Bases in the Solid State: Structural Aspects. Chem. Soc. Rev. 2004, 33, 579–588.

13. Jimenez-Sanchez, A.; Rodriguez, M.; Métivier, R.; Ramos-Ortiz, G.; Maldonado, J.L.; Rébolèes, N.; Farfán, R.; Nakatani, K.; Santillan, R. Synthesis and Crystal Structures of a Series of Schiff Bases: a Photo-, Solvato- and Acidochromic Compound. New. J. Chem. 2014, 38, 730-738.
14. Howard, J.A.K.; Probert, M.R. Cutting-Edge Techniques Used for the Structural Investigation of Single Crystals, Science 2014, 343, 1098-1102.
15. Carletta, A.; Dubois, J.; Tilborg, A.; Wouters, J. Solid-State Investigation on New Dimorphic Substituted N-Salicylidene Compound: Insights into its Thermochromic Behavior, CrystEngComm 2015, 17, 3509-3518.
16. Robert, F.; Naik, A. D.; Tinant, B.; Robiette, R.; Garcia, Y. Insights into the Origin of Solid-State Photochromism and Thermochromism of N-Salicylideneanils: The Intriguing Case of Aminopyridines. Chem. Eur. J. 2009, 15, 4327–4342.
17. Sliwa, M.; Naumov, P.; Choi, H.J.; Nguyen, Q.T.; Dubus, B.; Delbaere, S.; Ruckebusch, C. Effects of a Self-Assembled Molecular Capsule on the Ultrafast Photodynamics of a Photochromic Salicylideneaniline Guest, ChemPhysChem, 2011,12, 1669-1672.
18. Hutchins, K. M.; Dutta, S.; Loren, B. P.; MacGillivray, L. R. Co-Crystals of a Salicylideneaniline: Photochromism Involving Planar Dihedral Angles. Chem. Mater.2014, 26, 3042–3044.
19. Carletta, A.; Buol, X.; Leyssens, T.; Champagne, B.; Wouters, J. Polymorphic and Isomorphic Cocrystals of a N-Salicylidene-3-aminopyridine with Dicarboxylic Acids:Tuning of Solid-State Photo- and Thermochromism. J. Phys. Chem. C 2016, 120,10001–10008.
20. Ziolek, M.; Kubicki, J. ; Maciejewski, A. ; Naskrecki, R. ; Grabowska, A. Enol-Keto Tautomerism of Aromatic Photochromic Schiff Base N,N'-bis(Salicylidene)-pPhenylenediamine: Ground State Equilibrium and Excited State Deactivation Studied by Solvatochromic Measurements on Ultrafast Time Scale, J. Chem. Phys. 2006, 124,124518.
21. Bogdan, E., Plaquet, A., Antonov, L., Rodriguez, V., Ducasse, L., Champagne, B., Castet, F. Solvent Effects on the Second-Order Nonlinear Optical Responses in the Keto-Enol Equilibrium of a 2-Hydroxy-1-Naphthaldehyde Derivative. J. Phys. Chem.C 2010, 114, 12760–12768.
22. Sliwa, M.; Létard, S.; Malfant, I.; Nierlich, M.; Lacroix, P. G.; Asahi, T.; Masuhara, H.; Yu, P.; Nakatani, K. Design, Synthesis, Structural and Nonlinear Optical Properties of Photochromic Crystals: Toward Reversible Molecular Switches. Chem. Mater. 2005, 17, 4727–4735.
23. Ségerie, A., Castet, F., Kanoun, M. B., Plaquet, A., Liégeois, V., Champagne, B. Nonlinear Optical Switching Behavior in the Solid State: A Theoretical Investigation on Anils. Chem. Mater., 2011, 23, 3993–4001.
24. F. Castet and B. Champagne, Switching of the Nonlinear Optical Responses of Anil Derivatives: from Dilute Solutions to the Solid State, in Tautomerism: Concepts and Applications in Science and Technology, edited by L. Antonov, Wiley-VCH,Weinheim,2016, 175-202.
25. Antonov, L., Ed. Tautomerism: Methods and Theories; Wiley-VCH, Weinheim, 2013.

26. Antonov, L., Ed. Tautomerism: Concepts and Applications in Science and Technology; Wiley-VCH, Weinheim, 2016.
27. K. Boonkitpatarakul, J. Wang, N. Niamnont, B. Liu, L. Mcdonald, Y. Pang, M. Sukwattanasinitt,Novel turn-on fluorescent sensors with mega stokes shifts for dual detection of Al3+ and Zn2+, ACS Sens., 1 (2016) 144-150.
28. J. Zhao, S. Ji, Y. Chen, H. Guo, P. Yang, Excited state intramolecular proton transfer (ESIPT): from principal photophysics to the development of new chromophores and applications in fluorescent molecular probes and luminescent materials, Phys. Chem. Chem. Phys., 14 (2012) 8803-8817.
29. V.S. Padalkar, S. Seki, Excited-state intramolecular proton-transfer (ESIPT)-inspired solid state emitters, Chem. Soc. Rev., 2016,45,169.
30. G. W. T. M.J. Frisch, H.B. Schlegel, G.E. Scuseria, M.A. Robb, J.R. Cheeseman, G. Scalmani, V. Barone, B. Mennucci, G.A. Petersson, H. Nakatsuji, M. Caricato, X. Li, H.P. Hratchian, A.F. Izmaylov, J. Bloino, G. Zheng, J.L. Sonnenberg, M. Hada, M. Ehara, K. Toyota, R. Fukuda, J. Hasegawa, M. Ishida, T. Nakajima, Y. Honda, O. Kitao, H. Nakai, T. Vreven, J.A. Montgomery, Jr., J.E. Peralta, F. Ogliaro, M. Bearpark, J.J. Heyd, E. Brothers, K.N. Kudin, V.N. Staroverov, R. Kobayashi, J. Normand, K. Raghavachari, A. Rendell, J.C. Burant, S.S. Iyengar, J. Tomasi, M. Cossi, N. Rega, J. M. Millam, M. Klene, J.E. Knox, J.B. Cross, V. Bakken, C. Adamo, J. Jaramillo, R. Gomperts, R.E. Stratmann, O. Yazyev, A.J. Austin, R. Cammi, C. Pomelli, J.W. Ochterski, R.L. Martin, K. Morokuma, V.G. Zakrzewski, G.A. Voth, P. Salvador, J.J. Dannenberg, S. Dapprich, A.D. Daniels, O. Farkas, J.B. Foresman, J.V. Ortiz, J. Cioslowski, , D.J. Fox, , (Gaussian, Inc, Wallingford CT, 2009).
31. Andrienko, G. A. Chemcraft 1.8. website: http://www.chemcraftprog.com (Date of access: 08/08/2016) (2016).
32. Raghavachari, K. Perspective on “Density functional thermochemistry. III. The role of exact exchange” - Theor. Chem. Acc. 103, 361–363 (2000).
33. Miehlich, B., Savin, A., Stoll, H. & Preuss, H. Results Obtained with the Correlation-Energy Density Functionals of Becke and Lee, Yang and Parr. Chem. Phys. Lett. 157, 200–206 (1989).
34. Lee, C. T., Yang, W. T. & Parr, R. G. Development of the Colle-Salvetti Correlation-Energy Formula into a Functional of the Electron Density. Phys. Rev. B. 37, 785–789 (1988)
35. M. Petersilka, U. Gossmann and E. Gross, Physical review letters 76, 1212 (1996).
36. Krishnan, R., Binkley, J. S., Seeger, R. & Pople, J. A. Self-Consistent Molecular-Orbital Methods 20. Basis Set for Correlated WaveFunctions. J. Chem. Phys. 72, 650–654 (1980).
37. Cossi, M., Rega, N., Scalmani, G. & Barone, V. Energies, structures, and electronic properties of molecules in solution with the C-PCM solvation model. Journal of Computational Chemistry 24, 669–681 (2003).
38. Barone, V. & Cossi, M. Quantum calculation of molecular energies and energy gradients in solution by a conductor solvent model. J. Phys. Chem. A. 102, 1995–2001 (1998).

39. Lee, H., Hancock, R. D. & Lee, H. Role of Fluorophore – Metal Interaction in Photoinduced Electron Transfer (PET) Sensors: Time-Dependent Density Functional Theory (TDDFT) Study. Phys. Chem. A 2013, 117, 50, 13345.
40. Joseph W. Nugent, Hyunjung Lee, Hee-Seung Lee, Joseph H. Reibenspies and Robert D. Hancock, Chem. Commun., 2013,49, 97491.
41. Jiang P., Guo, Z. Fluorescent detection of zinc in biological systems: recent development on the design of chemosensors and biosensors; Coord. Chem. Rev. 248 (2004) 205.
42. Zang, D., Zheng, R., Wang, Y. & Lv, J. The ESIPT mechanism of dibenzimidazolo diimine sensor: A detailed TDDFT study. J. Phys. Org. Chem.2016, 29, 161.
43. Zhiyong Zhang,Chengjun Wang,Zhong zhiZhang,Yijing Luo,Shanshan Sun,Guangqing Zhang. Cd(II) enhanced fluorescence and Zn(II) quenched fluorescence with phenylenevinylene terpyridine: A theoretical investigation. Spectrochim. Acta - Part A Mol. Biomol. Spectrosc. 2019, 209, 40.

Figures

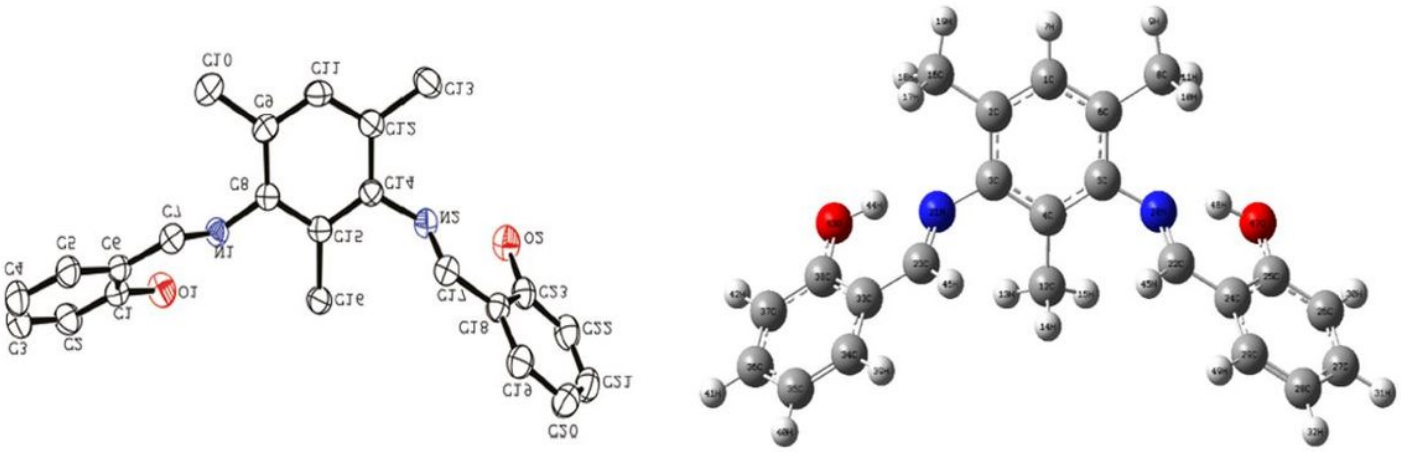

Figure 1

The atom numbering of E-cis H2L ligand optimized structure (Adopted from Ref. 1).

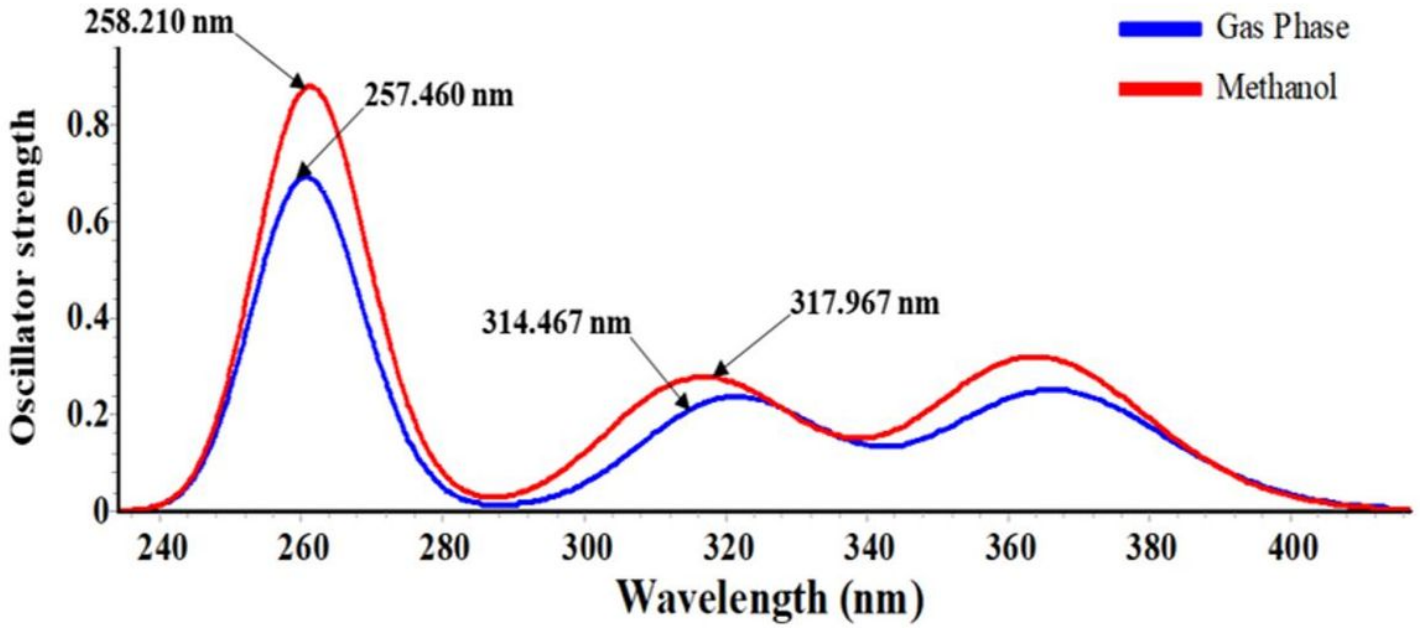

Figure 2

UV-Vis spectra of E-cis in the gas-phase and methanol obtained by using TDDFT/B3LYP/6-311++G** level of theory

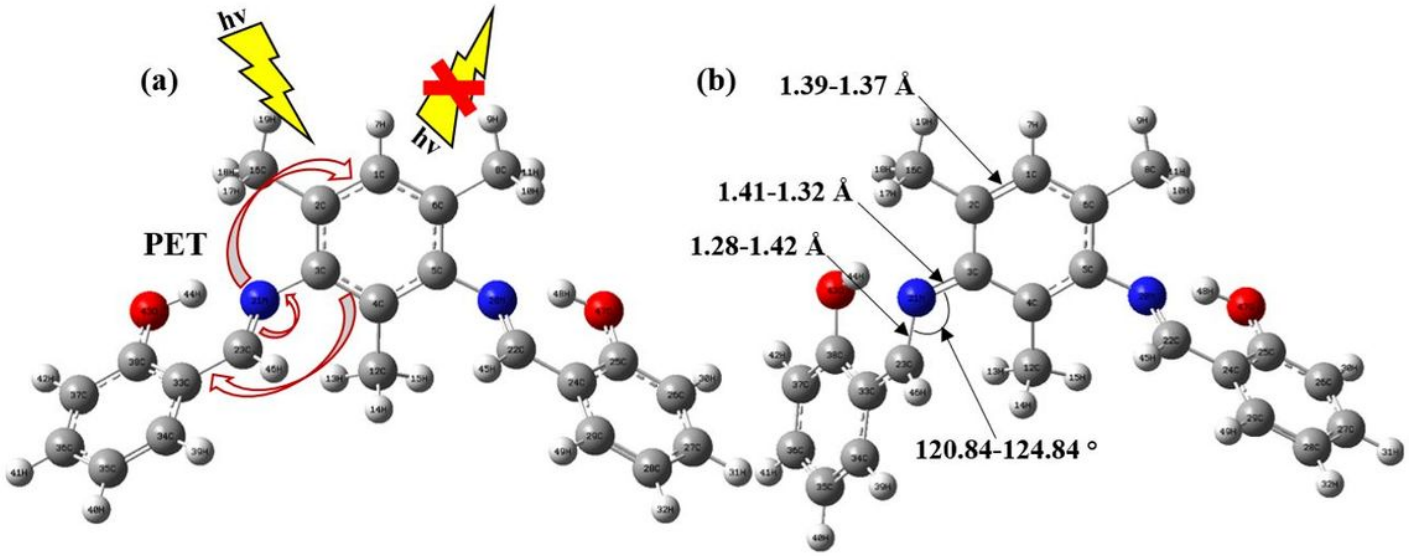

Figure 3

(a) The optimized structure of E-cis tautomer using DFT calculation and the display of PET mechanism occurring through photoexcitation (b) The effect of the PET mechanism on the structure of the E-cis tautomer resulted from the photoexcitation.

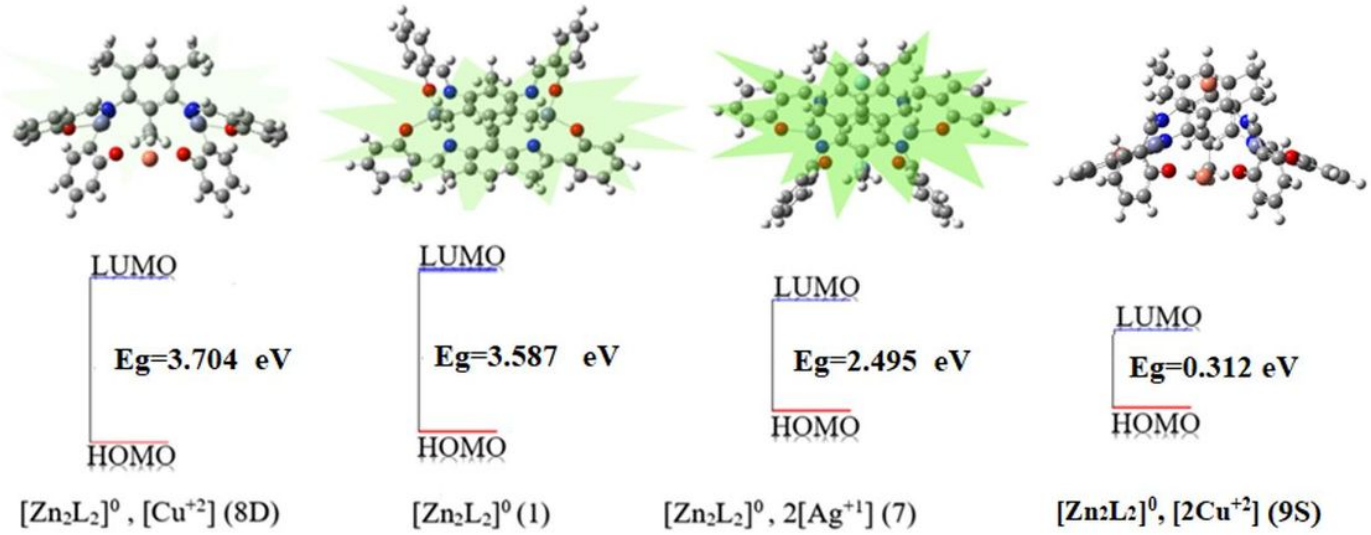

Figure 4

The blue/redshift leading to the absorption and emission spectra of the (8D), (9S) and (7) and the working principle of (Complex 1) as a fluorescent PCT sensor of the Cu2+ or Ag+ ion, by increasing/decreasing the energy gap as a result of the ICT mechanism using DFT/B3LYP/LANL2DZ/6-311++G** level of theory

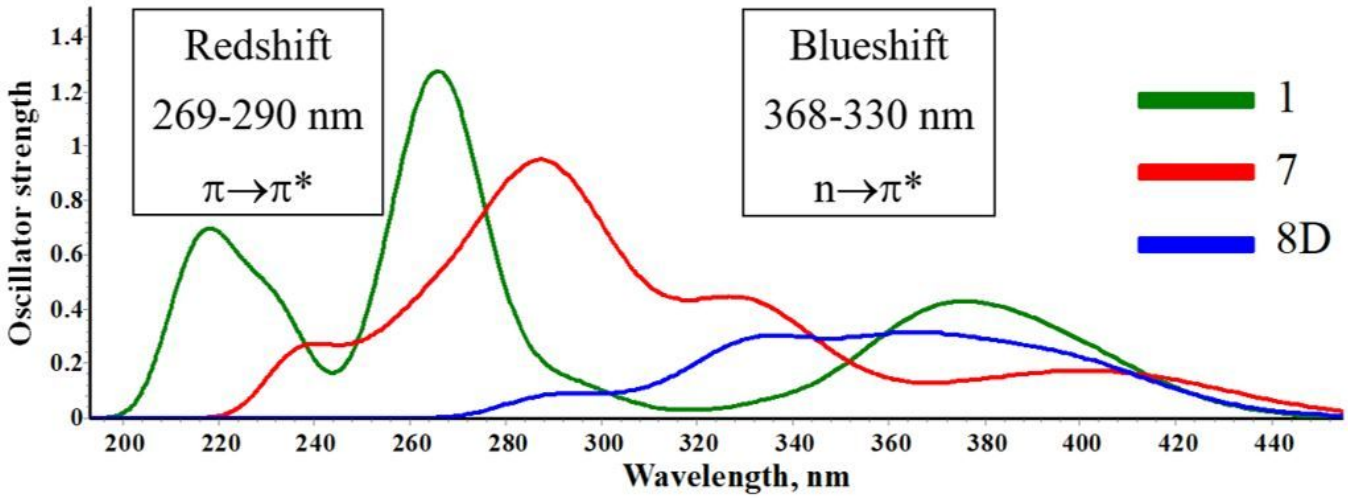

Figure 5

The simulated absorption spectra of complexes 1, 7 and 8D obtained by using B3LYP/LANL2DZ/6-311++G** level of theory.

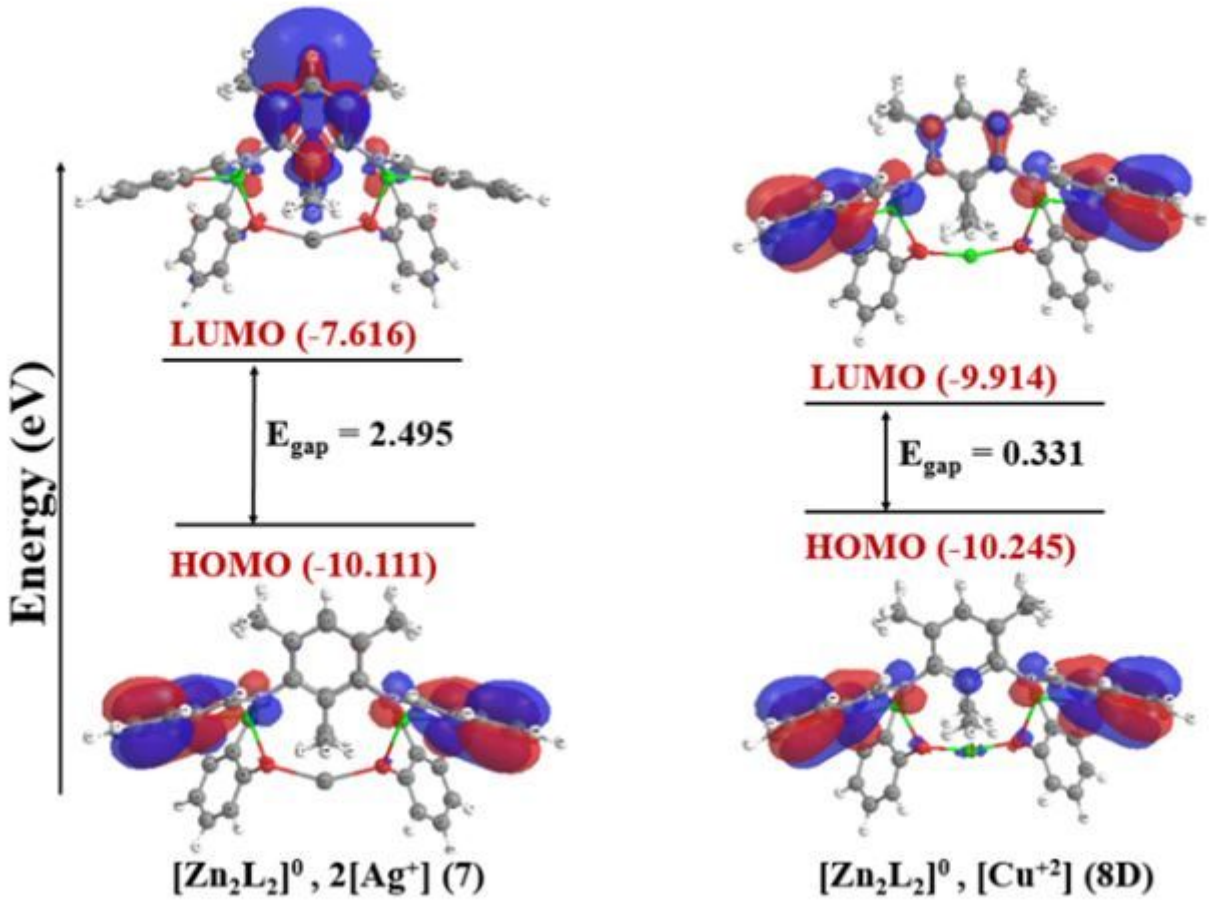

Figure 6

HOMO-LUMO and energy gaps of complex 7 {[Zn2L2]0, 2[Ag+]} and complex 8D {[Zn2L2]0, [Cu2+]} obtained by using TDDFT/B3LYP/LANL2DZ/6-311++G**) level of theory.

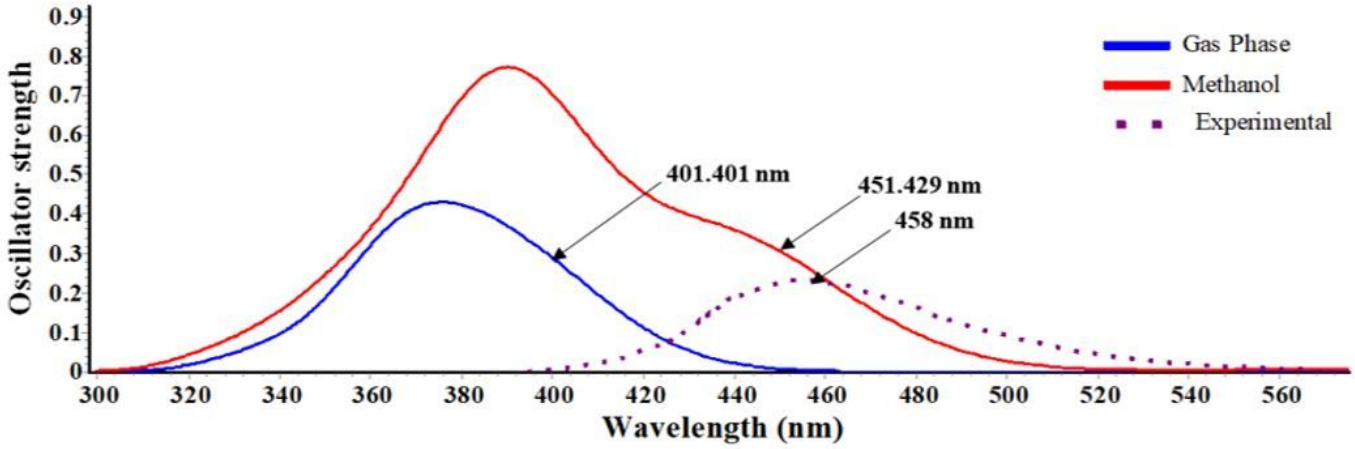

Figure 7

UV-Vis emission spectra of complex 1 obtained by using TDDFT/B3LYP/ LANL2DZ/6-311++G** level of theory in gas-phase and solution (methanol) together with experimental one for comparison purposes.

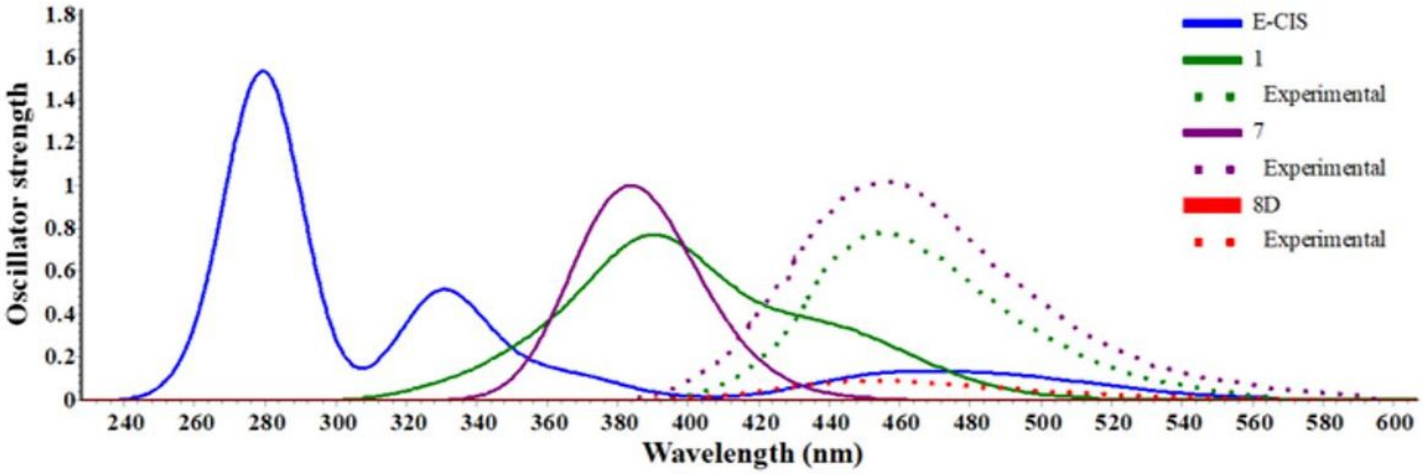

Figure 8

UV-Vis emission spectra of E-cis ligand and complexes 1, 7 and 8D in methanol as a solvent obtained by using TDDFT/B3LYP functional with 6-311++G** for ligand and LANL2DZ/6-311++G** basis set for the complexes.

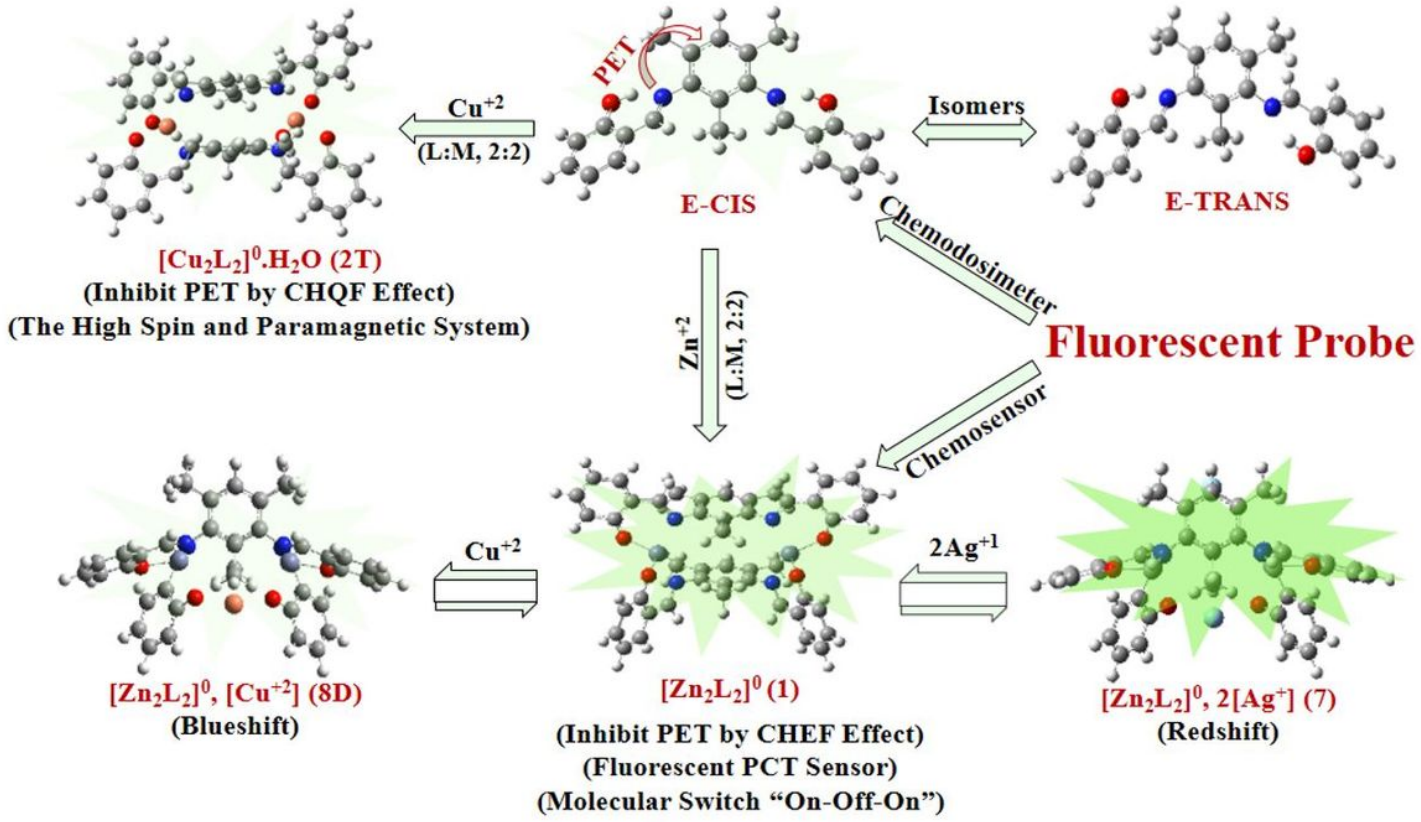

Figure 9

A summary illustrating the optimized structures of the most important substrates of the present work at B3LYP/ LANL2DZ/6-311++G** level of theory

Supplementary Files

This is a list of supplementary files associated with this preprint. Click to download.

- scheme1.jpg
- SupportingMaterials.docx